Delft University of Technology

Reliability Enhancement of Isolated Full-Bridge DC-DC Power Converter for Fast Charging of Electric Vehicles

Kardan, Faezeh; Shekhar, Aditya; Bauer, Pavol

DOI
10.1109/OJPEL.2024.3458813

Publication date
2024

Document Version
Final published version

Published in
IEEE Open Journal of Power Electronics

Citation (APA)
Kardan, F., Shekhar, A., & Bauer, P. (2024). Reliability Enhancement of Isolated Full-Bridge DC-DC Power Converter for Fast Charging of Electric Vehicles. *IEEE Open Journal of Power Electronics*, *5*, 1363-1374. https://doi.org/10.1109/OJPEL.2024.3458813

Important note
To cite this publication, please use the final published version (if applicable).
Please check the document version above.

Copyright
Other than for strictly personal use, it is not permitted to download, forward or distribute the text or part of it, without the consent of the author(s) and/or copyright holder(s), unless the work is under an open content license such as Creative Commons.

Takedown policy
Please contact us and provide details if you believe this document breaches copyrights.
We will remove access to the work immediately and investigate your claim.

This work is downloaded from Delft University of Technology.
For technical reasons the number of authors shown on this cover page is limited to a maximum of 10.

IEEE Open Journal of
Power Electronics

Received 10 July 2024; revised 25 August 2024; accepted 4 September 2024. Date of publication 11 September 2024;
date of current version 24 September 2024. The review of this article was arranged by Associate Editor Xiong Du.

Digital Object Identifier 10.1109/OJPEL.2024.3458813

Reliability Enhancement of Isolated Full-Bridge DC–DC Power Converter for Fast Charging of Electric Vehicles

FAEZEH KARDAN (Student Member, IEEE), ADITYA SHEKHAR (Member, IEEE), AND PAVOL BAUER (Senior Member, IEEE)

Department of Electrical Sustainable Energy, DCE&S Group, Delft University of Technology, 2628 CD Delft, The Netherlands

CORRESPONDING AUTHOR: FAEZEH KARDAN (e-mail: f.kardanhalvaei@tudelft.nl).

ABSTRACT In the realm of electric mobility, fast chargers for electric vehicles (EVs) play a critical role in mitigating range anxiety while driving. The converter in these chargers usually has a load profile consisting of a high-current pulse to swiftly recharge the EV battery, followed by a cooling-off phase when the charging process is over. This pattern results in thermal cycles on the devices resulting in mechanical fatigue that leads to gradual deterioration of the power electronic components. Consequently, evaluating the power electronic converters reliability is critical to facilitating fast EV charging. This paper focuses on the reliability analysis of the phase-shifted full-bridge DC/DC converter within EV fast chargers, with a specific emphasis on the battery charging profile. The primary objective is to demonstrate how the charger load characteristics and number of charging sessions influence device reliability and, consequently, overall system reliability. Additionally, the investigation explores the effects of altering devices heatsinks and current ratings on system reliability. It was observed that in worst-case scenarios, increasing devices current rates extended the system lifetime from 0.7 to about 23 years, with 3 p.u. ratings achieving 10.8 years, meeting industry targets, while reducing heatsink thermal resistance improves that to around 2 years.

INDEX TERMS EV charger, full-bridge DC/DC converter, lifetime, power components, reliability, thermal cycles.

I. INTRODUCTION

Reliability stands as a critical element impacting both the overall life-cycle expenses and the accessibility of power electronic systems. In recent years, the demand for higher reliability in power electronic applications has led to stricter lifetime constraints. This has resulted in increased efforts, such as testing, design, and analysis, during the early stages of development to meet these reliability requirements [1]. So the mission/load profile-based lifetime prediction technique for reliability is a methodology that has gained prominence in the last few years. For example, recent research on the wear-out failures of an impedance-source PV microinverter demonstrated the effectiveness of mission profile-based system-level electro-thermal modeling in identifying critical components, that significantly impact long-term reliability. The study proposed design improvements and advanced controls, emphasizing the role of thermal analysis and mission-specific profiling in enhancing reliability in harsh environments [2].

Power converters are relatively more vulnerable to failures during operation, thus significantly affecting the reliability of such systems [3]. According to studies, power switches and capacitors are the most failure-prone components of power electronic interfaces, PEIs, [4], [5], [6]. The reliability of power converters is substantially impacted by thermo-mechanical fatigues, which are the primary root of failures in power devices. Thermal stresses lead to these fatigues, which play a major role in wear-out failures. Research indicated that half of all stressors are thermal [7]. Power converters create power losses during their operation, making thermal cycles due to repeated heating and cooling triggered by load

© 2024 The Authors. This work is licensed under a Creative Commons Attribution-NonCommercial-NoDerivatives 4.0 License. For more information, see https://creativecommons.org/licenses/by-nc-nd/4.0/

variations, switching, and environmental situations. Given that power devices consist of multiple layers that vary in coefficients of thermal expansion, fluctuations in temperature may result in thermo-mechanical fatigue, which includes solder and bond-wire fatigue, as well as chip metallization degradation. All of these fatigues consume the life of the power semiconductors and power converters [8]. These thermal cycles that impact the converter reliability are separated into short-term, fundamental, from seconds to minutes, and long-term, from minutes to months, thermal cycles based on their duration [7]. The converter switching frequency is associated with short-term temperature fluctuations, whereas fundamental thermal cycles are caused by load variations. The long-term thermal cycle is impacted by environmental factors, including variations in the ambient temperature [7], [8]. The thermal capacitance of layers over the route of the power module operates like a kind of low-pass filter, mitigating the influence of thermal cycles near the heatsink that have a shorter duration or greater frequencies. Nevertheless, high-frequency fluctuations in temperatures have a more pronounced impact at the junction, leading to bondwire fatigue. On the other hand, longer-term temperature fluctuations have a consequence on the baseplate solder junction of the module [9]. The outcomes of power cycling experiments show that bond wires and die-attach solder wear out under short-term power cycles, while DBC-attach solder and the thermal interface also get fatigued over long-term power cycles [7], [10], [11]. In relation to aluminum electrolytic capacitors, inside hot-spot temperature and voltage stress are the primary stresses that cause wear-out failures and long-term degradation in these capacitors [12]. So these components significantly impact the reliability of the converter.

Off-board fast chargers are used for electric vehicles (EVs) while traveling over extended distances because of the limited capacity of on-board chargers. These chargers efficiently provide the necessary DC power to EV batteries using power converters and successfully prevail over the size and weight restrictions associated with on-board chargers. An EV can be fully charged in roughly 30 minutes using off-board chargers, with power levels ranging from 50 kW to 350 kW. Given the extra power conversion stages, AC-connected fast chargers become less efficient and more complicated than DC-connected fast chargers, albeit with some benefits such as protective devices, standardized protocols, and converter technology accessibility. Consequently, DC-fast chargers are more economically feasible, which also minimizes synchronization issues [13]. So, they are now at the forefront of charging technology, thanks to their advantages. To match the voltage needed for EV batteries while establishing galvanic isolation between the grid and the battery, isolated DC/DC converters are utilized in the second power transfer stage of DC fast chargers [13], [14]. In EV fast charging systems, the converter usually experiences a few minutes of high-current pulses to speed up the charging of EV batteries. After the charging process, the converter cools down. This cyclic activity exposes power electronic components to temperature cycles, potentially leading to their breakdown owing to mechanisms including thermo-mechanical fatigue [15], [16], [17]. Therefore, it's critical to evaluate power converters' reliability in EV fast charging applications according to their load profile. [18] highlights the critical importance of thermal dynamics in power semiconductors and capacitors for reliability assessments in power electronic converters. The study introduces a novel approach to evaluating converter-level reliability by simplifying models under a low sample rate mission profile for wind turbines, offering valuable insights that can be adapted to other applications. [7] explores how different thermal cycling scenarios impact the lifetime of power devices in wind turbine converters. By analyzing both fundamental-frequency and load-varying thermal cycles, the study provides crucial insights into the thermal stress factors that influence the reliability of power converters in renewable energy systems.

While extensive studies have done mission profile-based reliability assessments across a range of applications, including PV, wind, drive train, aerospace, and onboard chargers [18], [19], [20], there remains a gap in investigating reliability analysis based on the battery load in the context of DC fast chargers.

This study investigates the load-dependent reliability of an isolated phase-shifted full-bridge (PSFB) DC-DC converter, which is frequently used in EV fast chargers. Our research begins by leveraging validated models, which are based on experimental data related to device current ratings and blocking voltages, to precisely calculate power losses within the converter. Furthermore, the study explores the impact of the number of charging sessions on system reliability, a factor highly pertinent to the performance and reliability of EV fast chargers. By analyzing how the numbers of charging sessions influence the overall system reliability, the study offers valuable insights into this rapidly expanding field. Moreover, a comprehensive examination is conducted to see how the overall system reliability is affected by changes in heatsink thermal resistance and also device current rating. Even with a thorough investigation of reliability across a wide range of domains and applications, new technologies like EV fast charger applications present substantial obstacles that demand careful reliability analysis. This reliability study within the specific context of EV fast chargers—considering a unique load profile and operational scenarios— yields actionable insights that are crucial for enhancing reliability in real-world applications.

This paper is organized into the following sections: The process for assessing power converter reliability is described in Section II, with an emphasis on the load profile. We go into detail about the PSFB converter reliability in Section III, covering converter modeling, component power loss, temperature profiles, and system lifetime analysis. Section IV also explores the effects of modifying the heatsink and altering the devices current ratings. Finally, Section V presents the conclusions derived from the data.

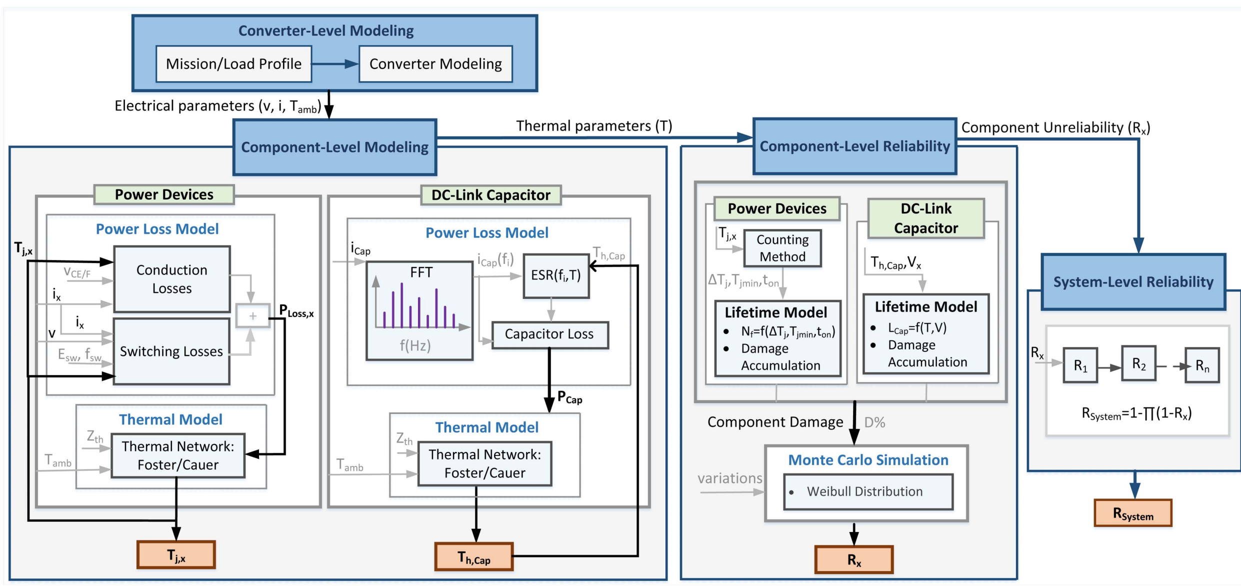

FIGURE 1. The methodology for mission/load-based reliability assessment of power converters.

II. LOAD-BASED RELIABILITY OF POWER CONVERTERS

A load/mission profile encompasses the key environmental and operational conditions that a system encounters during its lifetime [21]. Temperature is a common factor affecting most power electronics applications, while other environmental and operating states vary by application and may have a notable impact on the system reliability. As a result, the power converter lifetime varies depending on the application and load/mission profile, emphasizing the significance of reliability evaluations based on application or load/mission profile data. Mission/load profiles can be derived from actual field observations or estimated using generalized or pessimistic scenarios. Depending on the particular application, the timescale of this profile can vary from seconds to years.

The methodology for the mission/load-based reliability assessment of power converters is presented in this section and is shown in Fig. 1. In this figure, the primary step is to establish the load profile under the specific application. Subsequently, the converter is modeled to reflect the nuances of the application, the defined mission/load profile, the chosen converter topology, as well as the implemented control and modulation strategies. This phase, referred to as converter-level modeling, is critical as it facilitates the extraction of electrical stress parameters for each relevant component. These parameters are essential for the subsequent phase, to compute the losses associated with each component. The component current flow is denoted by i_x, while the v represents the voltage stress experienced by that component. Furthermore, T_{amb} represents the localized ambient temperature surrounding each component. Where x signifies the specific component. The secondary step of the reliability evaluation of power converters is component-level modeling, which is linked to different kinds of components. As previously outlined, power semiconductors and capacitors play vital roles in power converters. They are significantly prone to thermal stress due to the variations in load and environmental conditions in different applications [22], causing thermo-mechanical wear-outs. As a result, the reliability of power electronic converters is closely intertwined with the reliability of these constituent parts. At this point, the power losses for each component are calculated using the electrical stresses found in the preceding phase. These losses in power devices include conduction losses as well as losses incurred during switching in power devices (switching losses). Where $v_{CE/F}$ specifies the forward voltage of the power device. Also, E_{sw} represents the switching or reverse recovery energy of the power device, and f_{sw} is the switching frequency. Power losses of capacitors are caused by the ripple current passing through the capacitor and its equivalent series resistance (ESR), which depends on the operation frequency and hotspot temperature. Subsequently, the thermal profile of every component ($T_{j,x}$ and $T_{h,Cap}$), characterized by the power devices junction temperature and capacitors hotspot temperature profiles, are derived through the use of electro-thermal networks, such as Foster or Cauer models. These networks are tailored based on the components thermal properties. An enhanced thermal network is established by using the components thermal parameters, as well as the thermal resistance contributed by the thermal interface material, and the thermal resistance associated with the specifically designed heat sink. In this figure, the Z_{th} is the thermal impedance curve which refers to the thermal network of the component. These thermal networks use the power losses of the components as their input. In the load-based reliability evaluation procedure, the third phase is called component-level reliability. Similar to the preceding phase, this one concentrates on specific components. The components thermal load consisting of the junction temperature of power devices ($T_{j,x}$) and the hot-spot temperature of capacitors ($T_{h,Cap}$) that was retrieved

from the preceding step is now used as an input to calculate the components accumulated damage ($D(\%)$) and expected lifetime. To predict the expected lifetime of components the empirical lifetime models are used. Since gathering field data for reliability assessments takes many years, these models are among the strategies that have been suggested and validated to ascertain the components lifetime under thermal cycles [23], [24], [25]. These models account for elements that might impact the lifetime of the components and have been taken along during aging experiments. These elements consist of the thermal cycle amplitude and its minimum value (ΔT_{j}, T_{jmin}), and length of on-time (t_{on}) for power devices, and hot-spot temperature ($T_{\mathrm{h,cap}}$), and operational voltage (V_{x}) for capacitors. In some cases, power devices experience complex junction temperature profiles caused by fluctuations in load/mission characteristics in power electronic applications, creating challenges to correctly distinguish the various values during operation because of this intricacy. So, counting strategies such as the Rainflow method [26] are applied to determine the number of cycles in the particular T_{j} and T_{jmin}. The Miner rule is employed to calculate accumulated damage (D) according to the associated component damage. This allows for the initial end-of-life estimation of the components to be obtained [27]. In the last stage of component level reliability, some uncertainties are taken into account using a statistical Monte-Carlo method [28], and the component reliability function (R_{x}) is estimated by the Weibull cumulative distribution function [29]. In the concluding stage of the reliability assessment approach, System-level reliability is addressed. To evaluate the overall reliability of the power electronics converters or system (R_{System}), this phase attempts to combine the individual reliability metrics of each component. To achieve this, the method typically utilized is the reliability block diagram (RBD) technique [30]. The details of this process are presented in the rest of the paper.

III. RELIABILITY ASSESSMENT OF PSFB DC/DC CONVERTER IN EV FAST CHARGERS

As mentioned before, the phase-shifted full-bridge (PSFB) DC/DC converter is a commonly used isolated DC/DC converter that performs as an interface in DC fast charging stations for batteries in EVs. Consequently, a thorough investigation of the PSFB DC/DC converter reliability based on the considered load profile is conducted in this section.

A. PSFB CONVERTER MODEL BASED ON THE LOAD PROFILE

Modeling the power converters is the initial stage in evaluating the reliability of power converters, as was highlighted in the preceding section. First, the load profile of the converter, which is the profile used to charge a battery with a voltage of 400 V and a capacity of 50.36 kWh is taken into account for the PSFB DC/DC converter under study. The structure of the PSFB converter with the studied load profile is depicted in Fig. 2. The parameters for this converter are provided in Table 1.

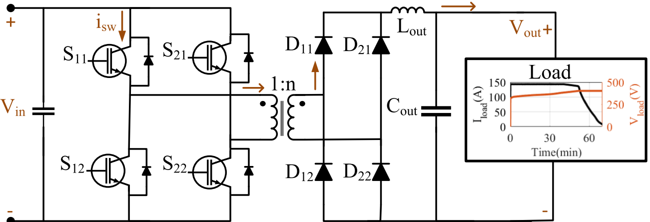

FIGURE 2. Structure of the isolated 55 kW PSFB DC/DC converter with the studied load profile used for EV charger.

TABLE 1. Specifications of the PSFB DC/DC

Converter parameters	Value
Rated power (P_{out})	55 kW
Output voltage (V_{out})	400 V
Switching frequency (f_{sw})	10 kHz
Input voltage (V_{in})	600 V
Inductance (L_{out})	0.25 mH
Capacitor (C_{out})	330 µF
Transformer ratio (n)	1 : 0.7

After analyzing and implementing the converter model in PLECS based on this load profile, the electrical stresses of the components are derived for use in the power loss calculations.

B. COMPONENTS POWER LOSS

The selection of components based on the predefined safety margins initiates the component-level modeling phase. The computation of each component power losses comes next. Thus, in the studied converter, the current ratings for IGBTs and diodes have been chosen as 100 A and 150 A for full-load operations, while the voltage ratings of 900 V and 600 V have been selected, respectively.

In this work, we apply the well-established models referenced in [31] to compute power device losses. This method estimates virtual power module losses while accounting for fluctuations in blocking voltage and rated current. Unlike other reliability studies that usually rely on device datasheets for power loss calculations, which may not always yield precise results, this method is both simpler and more accurate. The accuracy of this approach, validated through practical experiments as described by [31], enables a more precise estimation of losses, which is critical for a robust reliability assessment.

The presented models fit empirical data with physics-inspired models to evaluate the effect of blocking voltage and rated current on the losses encountered by IGBTs and diodes. Specifically, the method uses the proven linear relationship between the forward voltage drop and forward current for diodes and the collector-emitter voltage drop and collector current for IGBTs. Thanks to this methodology, loss calculations are ensured to reflect realistic performance parameters [31]. The collector-emitter voltage of the device against the collector current (i_{c}), denoted as ($v_{\mathrm{CE}}(i_{\mathrm{c}})$), can be

expressed as $v_{CE,0} + r.i_c$, based on the linear model presented in [31]. In this model, $v_{CE,0}$ represents the threshold or offset voltage, marking the point where the linear behavior begins in the output characteristic curve of the IGBT (V_{CE} vs. I_c curve). The parameter r is the slope of the linear portion of the curve, indicating the relationship between the voltage and the current in this region. Thus, the total forward voltage drop at the rated current (I_N) comprises two parts: $v_{CE,0}$ and $v_{CE,r}$, where $v_{CE,r}$ is equal to $r.I_N$. According to semiconductor physics [32], these parameters, as functions of the blocking voltage (V_B), namely $v_{CE,0}(V_B)$ and $v_{CE,r}(V_B)$, are described by (1), and (2). Consequently, the conduction loss of the device, $P_{cond,x}(V_B, I_N)$, for the examined IGBTs and diodes are computed depending on their V_B and I_N, as follows in (3) [31].

$$v_{CE,0}(V_B) = A_{v0} \cdot \log(B_{v0} \cdot V_B + C_{v0}) \tag{1}$$

$$v_{CE,r}(V_B) = r.I_N = A_r \cdot \log(B_r \cdot V_B). \tag{2}$$

$$P_{cond,x}(V_B, I_N) = v_{CE,0}(V_B) \cdot i_{x,avg} + r(V_B, I_N) \cdot i^2_{x,rms}. \tag{3}$$

Where A_{v0}, B_{v0}, C_{v0}, A_r, and B_r are constant parameters for the IGBT and diode models, as mentioned in [31]. These parameters were derived by fitting analytical expressions to empirical data from IGBTs, ensuring that the models accurately represent the relationship between the voltage drop and the blocking voltage. $i_{x,avg}$ and $i_{x,rms}$ are the average and RMS values of the device current.

To facilitate the depiction of switching losses in relation to the blocking voltage, the switching energies of individual devices have been calculated in proportion linearly with the switched current and the applied DC voltage (V_{dc}), this is represented as the blocking voltage utilization, u, shown in (4). So the switching and reverse recovery energy of the IGBTs and diodes, $E_{sw,rr}(V_B)$, and the switching loss of each device, $P_{sw,x}(V_B)$, based on the blocking voltage are calculated by (5), (6) [31].

$$u = \frac{V_{dc}}{V_B} \tag{4}$$

$$E_{sw,rr}(V_B) = K_{sw}(V_B) \cdot i_{x,avg} \cdot \frac{u}{0.5} \tag{5}$$

$$P_{sw,x}(V_B) = \frac{E_{sw,rr}(V_B) \cdot f_{sw}}{1000} \tag{6}$$

Where K_{sw} represents the normalized switching energy of the device which is estimated as follows in (7)–(10) [31]:

$$\begin{cases} K_{sw}(V_B)_{IGBT} = K_{OFF}(V_B) + K_{ON}(V_B) \\ K_{sw}(V_B)_{diode} = K_{rec}(V_B) \end{cases} \tag{7}$$

$$K_{OFF}(V_B) = A_{OFF}V_B^2 + B_{OFF}V_B + C_{OFF} \tag{8}$$

$$K_{ON}(V_B) = A_{ON}V_B^2 + B_{ON}V_B + C_{ON} \tag{9}$$

$$K_{rec}(V_B) = A_{rec}V_B^2 + B_{rec}V_B + C_{rec} \tag{10}$$

Where $K_{OFF}(V_B)$, $K_{ON}(V_B)$, and $K_{rec}(V_B)$ defined as approximated normalized turn-off, turn-on, and diode recovery energies as functions of the blocking voltage. A_{OFF}, B_{OFF}, C_{OFF}, A_{ON}, B_{ON}, C_{ON}, A_{rec}, B_{rec}, and C_{rec} are the constant parameters of IGBT and diode approximated models mentioned in [31] which were extracted by fitting models to empirical data.

Lastly, the conduction and switching losses will be added up to find the IGBTs and diodes overall power losses, $P_{Loss,x}$, which is shown in (11).

$$P_{Loss,x,IGBT/diode} = P_{cond,x}(V_B, I_N) + P_{sw,x}(V_B) \tag{11}$$

To estimate capacitor losses, the equivalent series resistor (ESR) which is the the primary cause of loss is used [33]. In this case study, the capacitor with Catalog-Part-Number 381LR331M450K052 is selected and its ESR is defined in its datasheet. So, (12) is used to calculate the capacitor total loss.

$$P_{Cap} = \sum_{i=1}^{n} ESR(f_i, T) \cdot i^2_{rms,Cap}(f_i) \tag{12}$$

Where $\mathrm{ESR}(f_i, T)$ refers to the capacitor ESR at the frequency f_i and temperature T and $i_{rms,Cap}(f_i)$ represents the RMS value of the ripple current across the capacitor at the same frequency, and n is the harmonic order.

C. THEMAL MODELLING OF THE COMPONENTS

At the end of the component-level modeling procedure, the thermal network of the elements is implemented to estimate the temperature profile, $T_{j,x}$ for the power devices and $T_{h,Cap}$ for capacitors. At this point, the thermal interface as well as heatsink thermal resistance (R_{ha}) for IGBTs and diodes should be used in conjunction with the devices thermal network. Thus, initially, the fair heatsinks should be designed for them. Since IGBTs and diodes face different electrical stresses in this study, these two types of devices are installed in two different heat sinks, with all IGBTs sharing one heat sink at the primary side and all diodes sharing another at the secondary side to determine the fair heat sinks. To establish the thermal networks of the components under study, firstly the junction-to-case thermal resistance of IGBTs and diodes (R_{JC}) concerning the specified V_B and I_N are calculated by the models provided in [31], as outlined in (13).

$$R_{JC}(V_B, I_N) = A_{Rth} \cdot (V_B \cdot I_N)^{-B_{Rth}} \tag{13}$$

Where A_{Rth} and B_{Rth} are the constant parameters of IGBT and Diode models mentioned in [31]. The resulting R_{JC} obtained from this model for studied IGBTs and diodes according to the ratings we selected, is 0.37 °C/W and 0.52 °C/W, respectively. Thus, by accounting for the thermal network where power losses act as the inputs which were extracted by (11), and (12), the temperature profile of each IGBT/diode ($T_{j,x}$) and capacitor ($T_{h,Cap}$) are estimated using (14), and (15), respectively.

$$T_{j,x} = P_{loss,x} \cdot R_{JC,x} + 4 \cdot P_{loss,x} \cdot (R_{cs} + R_{ha}) + T_{amb} \tag{14}$$

$$T_{h,Cap} = P_{Cap} \cdot (R_{hc} + R_{ca}) + T_{amb}. \tag{15}$$

Here, $R_{JC,x}$ is extracted using (13), while R_{CS} represents the thermal grease resistance, set at 0.005 °C/W. The heatsink

thermal resistance, R_{ha}, is designed to be 0.025 °C/W for IGBTs and 0.1 °C/W for diodes. Additionally, the ambient temperature (T_{amb}) is assumed to be 25 °C. This design ensures that the junction temperatures of both components are equivalent, resulting in a ΔT_j of 126 °C for both IGBTs and diodes. Additionally, R_{hc} and R_{ca} represent the thermal resistances of the chosen capacitor from the core to the bottom and from the case to the air, respectively. These values are specified as 8.82 °C/W and 4.48 °C/W, according to the selected capacitor's application guide.

D. LIFETIME ESTIMATION OF POWER COMPONENTS

In the process of power converters reliability evaluation, the subsequent stage following the determination of the temperature profile of components involves estimating their expected lifetime. This phase utilizes the components temperature data as a key input to compute power semiconductors number of cycles to failure (N_f) and capacitors lifetime (L_{Cap}) using established empirical lifetime models. Multiple lifetime prediction models for power devices, including LESIT, CIPS 2008 (Bayerer), corrected CIPS 2008, and the Skim models, which are all constructed around fundamental failure mechanisms, have been introduced in studies [23], [24], [25], [34], [35]. Features and details of these models are presented in [15], [21], [24], [34], [36]. The LESIT model overestimates cycles to failure in long-term heating due to its inability to consider cycle duration, which becomes critical for DBC solder joint fatigue. In contrast, the CIPS model and its corrected form, considering temperature swing length, provide a more precise estimation when DBC solder attach failure is the major cause of failure [15], [16]. Consequently, the chosen lifetime model should align with the temperature fluctuations period or be applicable to the specific application, corresponding to the most relevant failure mechanism [15], [16].

In EV fast chargers, the DBC-attached solder of power semiconductors gets influenced by thermal cycles because of the larger periods of temperature (t_{on}) [16]. The CIPS model, compared to its corrected model overestimates the N_f for elevated t_{on} values. This discrepancy arises because the DBC solder connection fails a few minutes after the heat hits the baseplate, indicating the device end of life [15]. To address this, the corrected CIPS lifetime model to estimate the number of cycles to failure is used, which is the more suitable model for EV charging applications. The CIPS and its corrected version are as follows [24], [34], [35] and shown in (16) and (17), respectively:

$$N_f = A \Delta T_j^{\beta_1} t_{on}^{\beta_3} I^{\beta_4} V^{\beta_5} D^{\beta_6} e^{\left(\frac{\beta_2}{T_{jmin}+273}\right)} \tag{16}$$

$$\frac{N_f(t_{on})}{N_f(1.5)} = \begin{cases} 2.25, & \text{if}\, t_{on} \leq 0.1\,\text{s}. \\ \left(\frac{t_{on}}{1.5}\right)^{-0.3}, & \text{if}\, 0.1 < t_{on} < 60\,\text{s}. \\ 0.33, & \text{if}\, t_{on} \geq 60\,\text{s}. \end{cases} \tag{17}$$

Where, N_f represents the number of cycles to failure in power devices, ΔT_j denotes the temperature cycles, T_{jmin} is the minimum junction temperature which is the ambient temperature in this study. Also, t_{on} refers to the heating time which is 4199.8 s in this study according to the load profile. The variables values, A, $\beta_1 - \beta_6$, are specified in [24]. Furthermore, I corresponds to the current per bond stitch, V indicates the device's voltage class ($V_B/100$), and D is the diameter of the bond wire in micrometers. The parameters of I, and D are assumed to be 20 A, and 250 μ, respectively. Thus, the $N_f(t_{on})$ for the IGBTs and diodes under study in the PSFB DC/DC converter according to the CIPS corrected model is predicted.

The 10-kelvin rule-which is derived from the Arrhenius law and is illustrated in (18) is the most commonly used lifetime model in the industry to predict the lifetime of the electrolytic capacitor [33].

$$L_{Cap} = L_0 \left(\frac{V_x}{V_0}\right)^{-n} 2^{\frac{T_0 - T_{h,Cap}}{10}} \tag{18}$$

Where L_{Cap} is the estimated lifetime of the capacitor, L_0 is the lifetime under test condition, n is defined in paper [33], V_x and V_0 are the voltage at the operational condition and rated voltage, respectively. T_0 and $T_{h,cap}$ are the hot-spot temperature of the capacitor at the operational and test conditions, respectively.

After estimating the $N_f(t_{on})$ in power devices and L_{Cap} of the capacitor by lifetime models, the accumulated damage is estimated Based on Miner's rule [27]. According to this rule, a power device becomes damaged due to the total of all thermal cycles, whereas damage to the capacitors is determined as the sum of the lifetime used up across sampling intervals. Consequently, the total accumulated damage of power devices and capacitor (D_{Device} and D_{Cap}) is written as in (19) [33]:

$$\begin{cases} D_{Device} = \sum_{j=1}^{n_D} \frac{n_j}{N_{fj}}, & \text{IGBT and diode} \\ D_{Cap} = \sum_{i=1}^{n_C} \frac{\Delta t}{L(T_{h,Cap})}, & \text{capacitor} \end{cases} \tag{19}$$

Where n_D represents the number of thermal cycles experienced by the power device over the year, n_j is the number of cycles occurring with the same thermal stress, N_{fj} refers to the number of cycles to failure at the j_{th} power cycle which is estimated by (17), in other words for each thermal cycle, there is a calculated number of cycles that a device can endure before it fails. n_c is the sampling points over the year, Δt is the load profile sampling interval, and $L(T_{h,Cap})$ comes from (18). This represents the lifetime of the capacitor at a given hot-spot temperature (T_h). The damage calculation in power devices and capacitors is based on the accumulation of stress over time, particularly through thermal cycles and operational conditions. For power devices, the damage is determined by summing the ratios of the number of thermal cycles experienced to the number of cycles to failure, considering the thermal stress each cycle imposes. For capacitors, damage is calculated by summing the fractions of the operational time over the expected lifetime, based on temperature and voltage conditions.

Finally, by summing the accumulated damage till it nears one, the components end-of-life, Lf, is determined by (20),

$$Lf_{\text{Device/Cap}} = \frac{1}{D_{\text{Device/Cap}}} \tag{20}$$

E. RELIABILITY FUNCTION OF THE POWER COMPONENTS

The end-of-life estimation of components in the previous part is based on the idealistic assumption that every component deteriorates at the same rate. However, real-world situations often generate uncertainty due to variations in the lifetime model parameters and discrepancies inherent in the component fabrication process. Therefore, this section is dedicated to exploring the components reliability while assuming these uncertainties. For this aim, the Monte Carlo method, which is a well-known statistical approach, is applied [28], providing a more thorough and realistic investigation of the components reliability under variable situations. Thus, the reliability assessment of the power component comes to an end at this stage, resulting in the determination of the component reliability function and the B_{10} lifetime. The B_{10} lifetime represents the time at which 10% of the components are expected to fail by taking uncertainty into account.

So, to accurately predict the lifetime of components, this research takes into account 5% variations associated with fixed variables such as β_1, L_0 and n, and a 10% variation for β_2 in the lifetime models. Additional uncertainties arise from the components fabrication procedure, particularly affecting the T_{jmin} and ΔT_{j}. Consequently, ΔT_{j} and T_{jmin} vary by 5% and 10%, respectively [24], [33].

Consequently, to drive the lifetime probability distribution function of each component, we employed the Monte Carlo method, simulating the component's lifetime based on the model as described in (20) of the previous section [28]. A total of 10,000 simulations were conducted to create a comprehensive probability distribution function in this simulation. The lifetime data for these components is assumed to follow the Weibull distribution [29], as expressed in (21). The reliability function of each component is subsequently derived from (22).

$$f(t) = \frac{\beta}{\eta}\left(\frac{t}{\eta}\right)^{\beta-1} e^{-\left(\frac{t}{\eta}\right)^{\beta}} \tag{21}$$

$$R_{\text{x}}(t) = 1 - \int_0^t f(t)dt = e^{-\left(\frac{t}{\eta}\right)^{\beta}} \tag{22}$$

Where η, and β are the scale parameter and shape factor of the Weibull distribution, respectively. η represents the characteristic life which provides a measure of the typical life expectancy of the component. β shapes the distribution, influencing the concentration and variability of failures.

As depicted in Fig. 3, the sets' estimated lifetimes of the analyzed components exhibit distinct Weibull distributions. It should be mentioned that the maximum number of charging sessions which is the worst case —15 per day—has been taken into consideration to extract the results in this section.

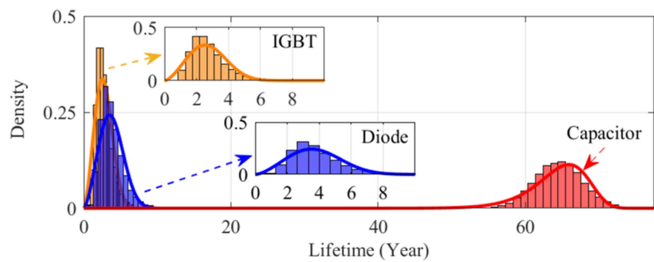

FIGURE 3. Monte Carlo simulations and Weibull distributions of components.

A higher η indicates that the failures occur later, shifting the entire distribution to the right. Conversely, a higher β results in a more concentrated distribution with less variability in time to failure meaning most components will fail around the same time. Fig. 3 illustrates that power devices (IGBTs and diodes) exhibit a more concentrated distribution with a lower scale parameter compared to capacitors. This is attributed to the higher thermal stress experienced by power devices, leading to shorter lifetimes. In contrast, capacitors show a more dispersed distribution with a higher scale parameter, indicating a longer expected lifetime with greater variability.

F. SYSTEM-LEVEL RELIABILITY OF PSFB CONVERTER

In the concluding phase of the reliability evaluation of the whole converter, which is called system-level reliability, the reliability block diagram, RBD, methodology is utilized [30]. This approach is essential for reliability analysis, particularly when dealing with multi-component systems. This method considers the impact of specific components on one another. The RBD for the studied converter is designed to include all IGBTs, all diodes, and the DC link capacitor based on the assumption that all components are arranged in a series configuration together. This specific arrangement is crucial, as it directly influences the reliability of the whole converter as the malfunction of a single component can precipitate a complete system failure. Equation (23) is used to quantify the system reliability.

$$R_{\text{System}} = R_1 \cdot R_2 \cdot R_3 \ldots R_n \tag{23}$$

Where R_{System} is the system Reliability, n represents the component, which is 9 in our case study, and R_{n} is the reliability of n_{th} component which were extracted in the previous part by (22).

Finally, the reliability function and B_{10} life of each component (IGBT, diode, and capacitor), as well as the entire system in our case study, were calculated using the (22), and (23) and are presented in Fig. 4. This reliability assessment method has been validated in the literature [3], [21], [29], [30].

According to Fig. 4, the IGBT and diode have a 1.3 and 1.8 years B_{10} life, respectively, while it's 59.3 years for the capacitor. As a result, the IGBTs and diodes are the main components affecting the system lifetime in this case study, which limits the system to having a B_{10} life of 0.7 a when

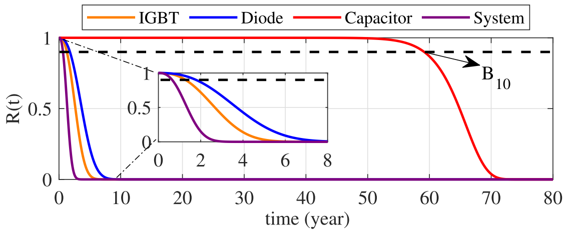

FIGURE 4. Reliability function of components and system.

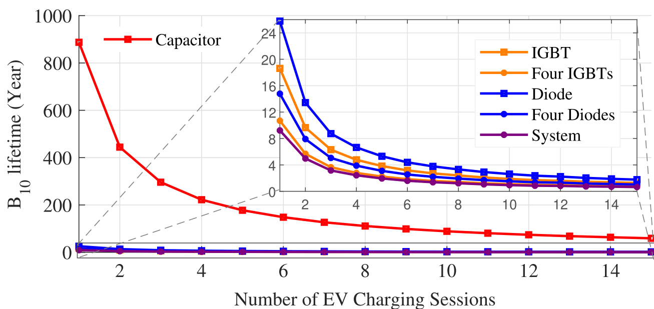

FIGURE 5. B_{10} **lifetime of the power devices, capacitor, and system in PSFB DC/DC converter based on the daily number of charging sessions.**

the maximum number of charging sessions (15 per day) is considered.

G. LIFETIME OF PSFB CONVERTER BASED ON THE NUMBER OF CHARGING SESSIONS

In this section, to guarantee that the T_j for both IGBTs and diodes are equal, the value of R_{ha} for IGBTs and diodes is taken to be the same as it was in the previous, that is, 0.025 °C/W and 0.1 °C/W, respectively. This assumption is applied to attain a ΔT_j of 126 °C for both devices. In this study, the components and system reliability are analyzed by considering the daily frequency of charging sessions, which varies between 1 and 15 times. This approach provides a comprehensive overview of the system reliability under different usage scenarios. As a result, the B_{10} life of components and system is predicted concerning the number of charging sessions, which are presented in Fig. 5. According to this figure, for a given number of charging sessions, the B_{10} life for a single diode is longer than that of a single IGBT. The reason for this discrepancy is attributed to the diode lower voltage class than the IGBT used in this specific converter. It is essential to acknowledge that the constant ΔT_j in both devices is the main stress that influences these outcomes. Also based on this curve, by considering a group of four IGBTs and diodes, the combined B_{10} lifetimes show a similar trend, albeit with a lower life. This highlights the influence that the number of devices has on the system overall reliability. In terms of the entire system B_{10} life, which integrates the reliability of all components, it follows a trend that is situated beneath those of the individual IGBTs and diodes. This indicates that the system overall reliability is impacted more by the weakest component. In other words, the capacitor does not influence the system reliability more. Additionally, the decrease in lifetime with an increased number of charging sessions emphasizes the significance of power cycling—represented by the charging frequencies of an EV on both the components and the system reliability. This underlines the necessity for a reliability assessment of EV fast chargers that takes into account the load profile.

IV. RELIABILITY ENHANCEMENT METHODS

A. IMPACT OF HEATSINKS MODIFICATION

In the next part of this study, we systematically reduced the heatsink thermal resistance, R_{ha}, for every IGBT and diode, intending to lower the ΔT_j, thereby enhancing the reliability of the devices. This reduction in thermal resistance of the heatsink can be achieved by modifying both the volume and surface area, as discussed in reference [31]. The thermal resistance of a heatsink is inversely proportional to its surface area—meaning that increasing the surface area improves the heatsink's efficiency in dissipating heat, which in turn lowers the thermal resistance. While the volume of the heatsink also influences thermal resistance, the relationship is more complex. A larger volume generally allows for better heat distribution, which can contribute to reducing thermal resistance. This approach allowed us to investigate the relationship between the R_{ha} and the ΔT_j, as well as the subsequent effects on devices and overall system reliability. So the IGBTs and the diodes respective R_{ha} is varied from 0.025 to 0.005 °C/W and 0.1 to 0.005 °C/W. Results are shown in Figs. 6 and 7.

Fig. 6 depicts the relationship between R_{ha}, ΔT_j, and component B_{10} life. Part (a) in this figure demonstrates how altering the R_{ha} affects the ΔT_j for both devices. It's shown that as the R_{ha} decreases, so does the ΔT_j for both devices. Parts (b), (c), and (d) demonstrate the effect of ΔT_j which corresponds to the R_{ha} on the B_{10} life of the devices for a fixed number of charging sessions, $n_{sessions} = 5$, 10, and 15. The B_{10} life for single and groups of four IGBTs and diodes are plotted against the ΔT_j. These figures illustrate a direct correlation between decreased ΔT_j and reduced R_{ha}, which adversely impacts the devices lifetime. However, the reliability improvement in IGBTs is not as substantial as it is for diodes, attributable to the greater losses experienced by IGBTs in the PSFB converter. As a result, the reduction in ΔT_j achieved by lowering the R_{ha} was more pronounced for diodes—with a decrease from 126 °C to 75 °C—compared to IGBTs, where the ΔT_j was lowered to 106 °C. Consequently, decreasing the R_{ha} caused a significant rise in the diodes B_{10} life, up to approximately 18 years, while the IGBTs B_{10} life rose to around 3 years under the worst scenario. Fig. 7 shows a detailed study of how the R_{ha} for both devices correlates with the B_{10} life of the system, carried out across a variety of $n_{sessions}$— 5, 10, and 15 cycles per day. A comparative evaluation of these plots shows that the high number of charging sessions shortens system B_{10} life. There is a noticeable gradient difference from the bottom left corner to the top

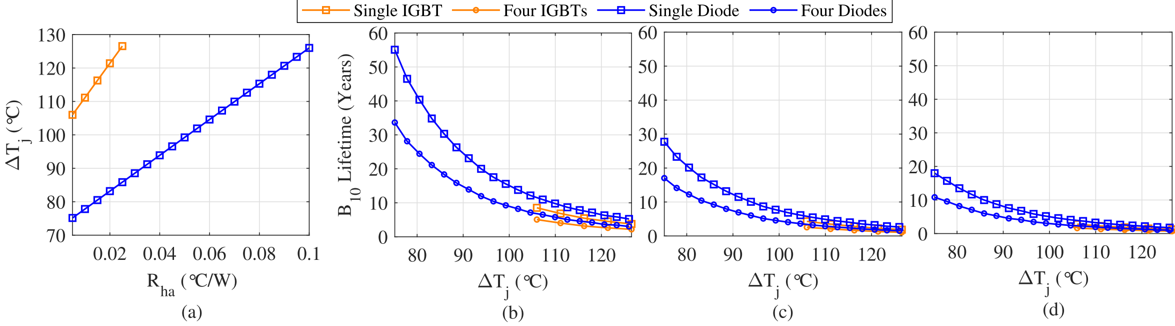

FIGURE 6. ΔT_j and B_{10} life of IGBTs and diodes by changing their heatsink thermal resistance, (R_{ha}), (a) devices ΔT_j, (b) devices lifetime when daily $n_{sessions}$ is 5, (c) devices lifetime when daily $n_{sessions}$ is 10, (d) devices lifetime when daily $n_{sessions}$ is 15.

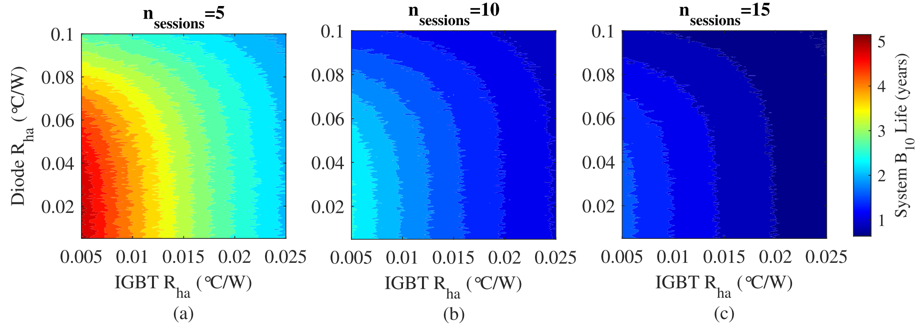

FIGURE 7. System B_{10} life based on the thermal resistance of heatsinks, (R_{ha}), (a) daily $n_{sessions}$ is 5, (b) daily $n_{sessions}$ is 10, (c) daily $n_{sessions}$ is 15.

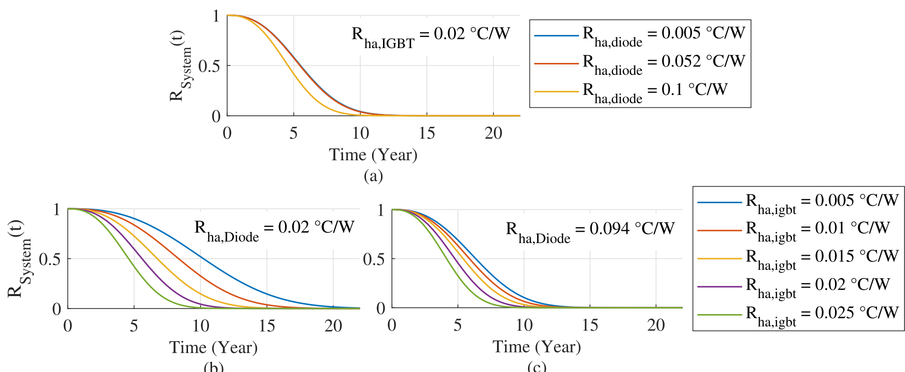

FIGURE 8. $R_{System}(t)$ based on the heatsink thermal resistance (R_{ha}) when daily $n_{sessions}$ is 5, (a) when diode (R_{ha}) is changing and $R_{ha,IGBT} = 0.02\,^\circ$C/W, (b) when IGBT R_{ha} is changing and $R_{ha,Diode} = 0.02\,^\circ$C/W, (c) when IGBT R_{ha} is changing and $R_{ha,Diode} = 0.094\,^\circ$C/W.

right corner, which shows that a reduction in the R_{ha} of both devices is associated with a higher system B_{10} life. According to Fig. 7(a), the system B_{10} life increased from 0.7 to 5 years by reducing the IGBT R_{ha} to $0.005\,^\circ$C/W and the diode R_{ha} to $0.04\,^\circ$C/W. The contour line distribution points to that at higher IGBT R_{ha} values, the system-level B_{10} life experiences minimal improvement, despite reductions in diode R_{ha}. This pattern underscores that the IGBT is the most fragile part of this case study, potentially limiting the system lifetime under certain conditions. Accordingly, a reduction in the IGBTs R_{ha} greatly extends the system life, which demonstrates the IGBTs substantial influence on overall system reliability. These insights emphasize the importance of the thermal design approach, with a special focus on designing IGBT heatsink thermal resistance. Additionally, when diode R_{ha} values are extremely high, a reduction in IGBT R_{ha} results in only a marginal increase in system reliability. However, the diode does not limit the system lifetime to the same extent as the IGBT. This emphasizes the need for heatsink design for both devices to achieve optimal system reliability. It's worth noting that since the capacitor has a longer lifetime than power devices under all conditions in this case, its lifetime does not influence the overall system lifetime. Detailed results that confirm the contour plots shown in Fig. 7 are presented in Fig. 8. According to Fig. 8(a), initially, the system lifetime improves as the diode R_{ha} is reduced from its maximum

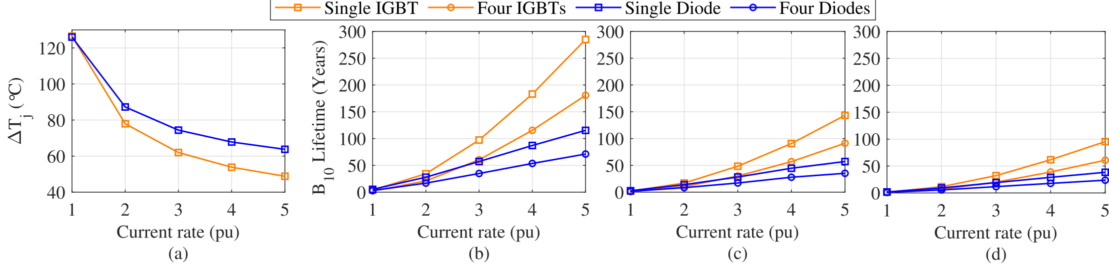

FIGURE 9. Power devices ΔT_j and B_{10} life based on the current rating for the different numbers of charging sessions. (a) Devices ΔT_j, (b) devices lifetime when the daily $n_{sessions}$ is 5, (c) devices lifetime when the daily $n_{sessions}$ is 10, (d) devices lifetime when the daily $n_{sessions}$ is 15.

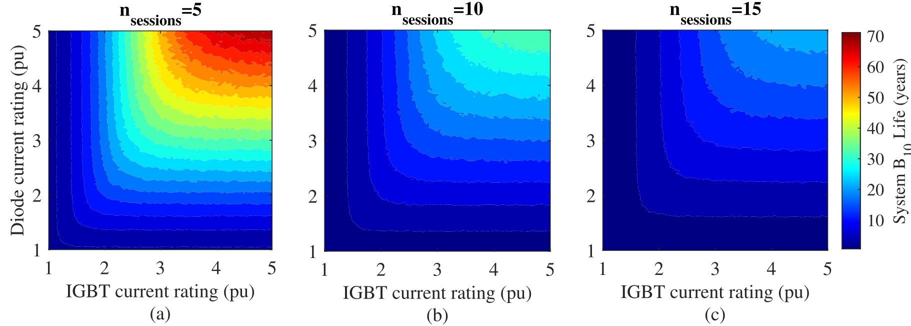

FIGURE 10. System B_{10} life based on the devices current rates at several numbers of charging sessions per day, 5, 10, and 15.

value. However, further reduction in diode R_{ha} does not yield additional enhancements in system lifetime. As previously mentioned, this effect arises since the IGBT R_{ha} is not as low, thereby limiting the total system lifetime. Fig. 8(b) shows that the reduction in the IGBT R_{ha} more effectively improves the system life when diode R_{ha} is not at its maximum value. Furthermore, Fig. 8(c) indicates that the decrease in IGBT R_{ha} only marginally extends the system life when the diode R_{ha} is too high.

B. IMPACT OF DEVICES CURRENT RATING

Similar to the previous section objectives, this section aims to investigate the impact of increased current ratings of devices on their and system reliability. It is noteworthy that the heatsink structures remain unchanged and mirror those employed in the first phase of the earlier section, $R_{ha,\,IGBT} = 0.025\,^{\circ}C/W$ and $R_{ha,\,Diode} = 0.1\,^{\circ}C/W$. This allows for a more straightforward reliability analysis when adjusting both the R_{ha} and the device current ratings. As a result, ΔT_j for both devices is 126°C in the initial phase of this section. So this stage of the study involves increasing the current ratings for each power device to reduce the ΔT_j and, as a result, improve devices reliability. This approach gives insight into how the devices current rates influence ΔT_j, which then affects the reliability of individual parts as well as the system as a whole.

To implement this approach during the reliability assessment process outlined in Fig. 1, IGBT and diode current ratings were varied between 100–500 A and 150–750 A, respectively. This variation was applied at the component level stage to calculate the corresponding losses, which naturally change with different current ratings. Subsequently, the ΔT_j range for each device, based on these ratings, was estimated using the thermal network model shown in Fig. 9. It is important to note that this temperature range arises from the variations in R_{JC} and power losses associated with the different current ratings. Finally, using the lifetime model and Monte Carlo simulations, as described in previous sections, we extracted the contour lines of the system-level B_{10} life for each device's current rating, as illustrated in Fig. 10.

The results of these changes are shown in Fig. 9 emphasizing the relationship between the devices ΔT_j and their current ratings, expressed in per units.

By raising the current ratings of both devices, we saw a decrease in the ΔT_j in Fig. 9(a). Subsequently, parts (b), (c), and (d) in this figure, explore the effects of these changes in ΔT_j, linked to the devices increased current ratings, on their B_{10} life across a fixed number of charging sessions, $n_{sessions}$ = 5, 10, and 15. Based on this figure, it is evident that the lifetime for both single devices and device groups increases with an increase in current ratings, highlighting a relatively higher reliability improvement for IGBTs compared to diodes. Since diodes only experienced a drop to 63.8 °C, IGBTs had a more significant decrease in ΔT_j through increased current ratings, going from 126 °C to 48.8 °C. This increase in current ratings substantially extended the B_{10} life of all IGBTs and diodes to approximately 60 and 24 years, respectively, which is shown in Fig. 9(d). Moreover, a comparative analysis with an earlier approach indicates that the devices current rating enhancement has a greater influence on improving device reliability than lowering the heatsink thermal resistance. Fig. 10 indicates a detailed analysis of the relationship between the devices current ratings and the system resulting B_{10} life,

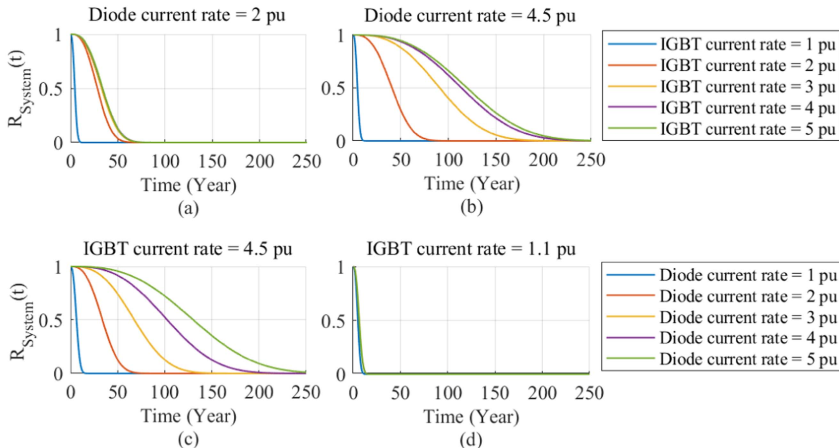

FIGURE 11. System reliability function, $R_{\mathrm{System}}(t)$, based on the devices current rating when the daily n_{sessions} is 5, (a) $R_{\mathrm{System}}(t)$ when IGBT current rating is changing and diode current rate = 2 p.u., (b) $R_{\mathrm{System}}(t)$ when IGBT current rating is changing and diode current rate = 4.5 p.u., (c) $R_{\mathrm{System}}(t)$ when diode current rating is changing and IGBT current rate = 4.5 p.u., (d) $R_{\mathrm{System}}(t)$ when diode current rating is changing and IGBT current rate = 1.1 p.u..

across different charging sessions specifically, 5, 10, and 15. Similar to Fig. 7, these plots show that a higher number of charging sessions leads to a lower B_{10} life of the system. Additionally, an adverse correlation between the higher current ratings and the decrease in ΔT_{j} causes a significant influence on the system lifetime. In this figure, a gradient transition from the bottom left to the top right corner is observable, indicating that an increase in current ratings extends the B_{10} life of the system due to the reduction in ΔT_{j} for both devices. Specifically, based on Fig. 10(a), by increasing the current ratings of both devices to 5 p.u., the system B_{10} life experiences a significant increase from 2 to 70 years. As well in the worst case the B_{10} life of system increased from 0.7 to about 23 years which is shown in Fig. 10(c). Additionally, as shown in Fig. 10(c), when the current rate of both devices is increased to 3 p.u., the system's B_{10} life extends to approximately 10.8 years, aligning with the industry target lifetime for EV fast-charging applications. According to the contour line distribution in this figure, the system reliability increase is more noticeable by IGBTs overrating than in diodes due to the greater changes in the junction temperature of IGBTs compared to the diodes. In other words, when the diode current rating is low, increasing the IGBT current rating does not significantly lengthen the system lifetime because the diode junction temperature fluctuates less than that of IGBT which limits the system life by diodes. These results emphasize the significance of current ratings in managing thermal performance and ensuring system reliability. Refined results verifying the contour analysis shown in Fig. 10 are demonstrated in Fig. 11, which presents system-level reliability functions. In Fig. 11(a), we see an initial improvement in the system reliability with increases in the IGBT current rating from its smallest values. However, further enhancements in system reliability are not presently possible with the next rise in the IGBT current rating. As previously mentioned, this is caused by the diode comparatively lower current rating, which operates as a limitation for the system total lifetime. As Fig. 11(b) shows, raising the IGBT current rating together with the diode higher current rate significantly boosts system reliability. This pattern occurs as well when the diode current rate rises along with higher IGBT current ratings, as illustrated in Fig. 11(c), highlighting the point that enhancing the current ratings of both devices greatly improves system reliability. Moreover, Fig. 11(d) shows that raising the diode current rating only marginally increases the system reliability when the IGBT current rating stays low as well, pointing out that the IGBT poses a greater limitation on the system reliability due to its higher power losses in this current rating. When these two approaches are compared, it is obvious that applying the current rating modification strategy eliminates the IGBT as a limiting factor for system reliability. This is because variations in power losses and thermal resistances arise from changing the current rate. Conversely, in the first approach—the modification of heatsink thermal resistance—device power losses were constant, and in the case of IGBTs, they were higher than the diodes, which limited the system lifetime.

V. CONCLUSION

This paper delves into the load-based reliability analysis of a 55 kW isolated phase-shifted full-bridge, PSFB, DC-DC converter in EV fast chargers, paying special attention to the issues of thermal cycling posed during charging. In this research, we investigated how different heatsink thermal resistance and device current ratings influenced the overall converter reliability. We calculated the power losses for each IGBT and diode using the presented experimental models, which offer a more accurate estimation of losses compared to traditional methods that rely solely on the device datasheet information. The components' lifetime has been estimated by proposed experimental-based lifetime models and the Monte Carlo simulation has been used to ensure accurate lifetime predictions to consider uncertainties. Our findings illustrate the necessity of load profile-based reliability assessment in DC fast charging and highlight the substantial impact of

temperature cycles characteristic of EV charging on device reliability. According to the observations, capacitors last longer than other parts. Additionally, results illustrated that the number of charging periods significantly affects the lifetime of the components and then the system. Moreover, results suggest that changing heatsink thermal resistance and current rating of power devices can lengthen the B_{10} life of the system, from 0.7 years to about 2 years due to decreased heatsink thermal resistance, and up to approximately 23 years because of raised device current ratings in a worst-case scenario with 15 daily charging sessions. Additionally, the lifetime can be increased to around 3 years due to decreased heatsink thermal resistance and up to approximately 35 years with higher device current ratings assuming 10 daily charging sessions. In conclusion, the current rating modification strategy effectively eliminates the IGBT as a limiting factor for system reliability by addressing variations in power losses and device thermal resistance. In contrast, in the heatsink modification approach, power losses remain constant and are higher for IGBTs compared to diodes, thereby limiting the system lifetime. However, it is important to consider these trade-offs between cost, efficiency, size, and increased system reliability.

REFERENCES

[1] Z. Chen et al., "Reliability-oriented multiobjective optimization of electrical machines considering insulation thermal lifetime prediction," *IEEE Trans. Transp. Electrific.*, vol. 10, no. 1, pp. 2264–2276, Mar. 2024.

[2] Y. Shen, A. Chub, H. Wang, D. Vinnikov, E. Liivik, and F. Blaabjerg, "Wear-out failure analysis of an impedance-source PV microinverter based on system-level electrothermal modeling," *IEEE Trans. Ind. Electron.*, vol. 66, no. 5, pp. 3914–3927, May 2019.

[3] S. Peyghami, P. Palensky, and F. Blaabjerg, "An overview on the reliability of modern power electronic based power systems," *IEEE Open J. Power Electron.*, vol. 1, pp. 34–50, 2020.

[4] S. Yang, A. Bryant, P. Mawby, D. Xiang, L. Ran, and P. Tavner, "An industry-based survey of reliability in power electronic converters," *IEEE Trans. Ind. Appl.*, vol. 47, no. 3, pp. 1441–1451, May/Jun. 2011.

[5] S. Yang, D. Xiang, A. Bryant, P. Mawby, L. Ran, and P. Tavner, "Condition monitoring for device reliability in power electronic converters: A review," *IEEE Trans. Power Electron.*, vol. 25, no. 11, pp. 2734–2752, Nov. 2010.

[6] D. Hirschmann, D. Tissen, S. Schroder, and R. W. D. Doncker, "Reliability prediction for inverters in hybrid electrical vehicles," *IEEE Trans. Power Electron.*, vol. 22, no. 6, pp. 2511–2517, Nov. 2007.

[7] G. Zhang, D. Zhou, J. Yang, and F. Blaabjerg, "Fundamental-frequency and load-varying thermal cycles effects on lifetime estimation of DFIG power converter," *Microelectronics Rel.*, vol. 76/77, pp. 549–555, 2017.

[8] K. Ma, M. Liserre, F. Blaabjerg, and T. Kerekes, "Thermal loading and lifetime estimation for power device considering mission profiles in wind power converter," *IEEE Trans. Power Electron.*, vol. 30, no. 2, pp. 590–602, Feb. 2015.

[9] F. Carastro, A. Castellazzi, J. Clare, and P. Wheeler, "High-efficiency high-reliability pulsed power converters for industrial processes," *IEEE Trans. Power Electron.*, vol. 27, no. 1, pp. 37–45, Jan. 2012.

[10] Y. Shi, J. Liu, Y. Ai, S. Chen, and C. Pei, "Lifetime prediction method of the traction converter IGBT based on plastic strain energy density," *IEEE Trans. Transp. Electrific.*, vol. 10, no. 1, pp. 1286–1298, Mar. 2024.

[11] M. Molenaar, F. Kardan, A. Shekhar, and P. Bauer, "Power and thermal cycling testbed for end of life assessment of semiconductor devices," in *Proc. IECON 2023- 49th Annu. Conf. IEEE Ind. Electron. Soc.*, 2023, pp. 1–6.

[12] R. Alwitt and R. Hills, "The chemistry of failure of aluminum electrolytic capacitors," *IEEE Trans. Parts, Mater., Packag.*, vol. PMP-1, no. 2, pp. 28–34, Sep. 1965.

[13] S. Srdic and S. Lukic, "Toward extreme fast charging: Challenges and opportunities in directly connecting to medium-voltage line," *IEEE Electrific. Mag.*, vol. 7, no. 1, pp. 22–31, Mar. 2019.

[14] S. G. Liasi, F. Kardan, and M. T. Bina, *Power Electronics Converters for EVs and Wireless Chargers: An Overview on Existent Technology and Recent Advances*. Hoboken, NJ, USA: Wiley, 2022, ch. 14, pp. 475–517.

[15] F. Kardan, A. Shekhar, and P. Bauer, "Quantitative comparison of the empirical lifetime models for power electronic devices in EV fast charging application," in *2023 11th Int. Conf. Power Electron. ECCE Asia*, 2023, pp. 3239–3244.

[16] F. Kardan, M. Ahmadi, A. Shekhar, and P. Bauer, "Load profile based reliability assessment of IGBT module in full-bridge DC/DC converter for fast charging of EVs," in *2023 25th Eur. Conf. Power Electron. Appl.*, 2023, pp. 1–8.

[17] F. Kardan, A. Shekhar, and P. Bauer, "End-of-life comparison of full-bridge and half-bridge DC/DC converter switches used for EV charging," in *Proc. IECON 2023- 49th Annu. Conf. IEEE Ind. Electron. Soc.*, 2023, pp. 1–6.

[18] D. Zhou and F. Blaabjerg, "Converter-level reliability of wind turbine with low sample rate mission profile," *IEEE Trans. Ind. Appl.*, vol. 56, no. 3, pp. 2938–2944, May/Jun. 2020.

[19] F. Blaabjerg, H. Wang, I. Vernica, B. Liu, and P. Davari, "Reliability of power electronic systems for EV/HEV applications," *in Proc. IEEE*, vol. 109, no. 6, pp. 1060–1076, Jun. 2021.

[20] F. Chan and H. Calleja, "Reliability estimation of three single-phase topologies in grid-connected PV systems," *IEEE Trans. Ind. Electron.*, vol. 58, no. 7, pp. 2683–2689, Jul. 2011.

[21] S. Peyghami, H. Wang, P. Davari, and F. Blaabjerg, "Mission-profile-based system-level reliability analysis in DC microgrids," *IEEE Trans. Ind. Appl.*, vol. 55, no. 5, pp. 5055–5067, Sep./Oct. 2019.

[22] J. Falck, C. Felgemacher, A. Rojko, M. Liserre, and P. Zacharias, "Reliability of power electronic systems: An industry perspective," *IEEE Ind. Electron. Mag.*, vol. 12, no. 2, pp. 24–35, Jun. 2018.

[23] M. Held, P. Jacob, G. Nicoletti, P. Scacco, and M. Poech, "Fast power cycling test of IGBT modules in traction application," in *Proc. Second Int. Conf. Power Electron. Drive Syst.*, Singapore, 1997, vol. 1, pp. 425–430.

[24] R. Bayerer, T. Herrmann, T. Licht, J. Lutz, and M. Feller, "Model for power cycling lifetime of IGBT modules - various factors influencing lifetime," in *Proc. 5th Int. Conf. Integr. Power Electron. Syst.*, Germany, 2008, pp. 1–6.

[25] U. Scheuermann and R. Schmidt, "A new lifetime model for advanced power modules with sintered chips and optimized AI wire bonds," in *Proc. PCIM Europe*, Nuremberg, 2013, pp. 810–817.

[26] H. Okamura, S. Sakay, and I. Susuki, "Cumulative fatigue damage under random loads," *Fatigue Fracture Eng. Mater. Structures*, vol. 1, no. 4, pp. 409–419, 1979.

[27] M. A. Miner, "Cumulative damage in fatigue," *J. Appl. Mechan.*, vol. 12, no. 3, pp. 159–164, 1945.

[28] J. McPherson, *Reliability Physics and Engineering*, 2nd ed. Cham, Switzerland: Springer, 2013.

[29] W. Weibull, "Statistical distribution function of wide applicability," *ASME J. Appl. Mechan.*, vol. 18, no. 3, pp. 293–297, Sep. 1951.

[30] R. Billinton and R. N. Allan, *Reliability Evaluation of Engineering Systems: Concepts and Techniques*. New York, NY, USA: Springer, 1992.

[31] J. E. Huber and J. W. Kolar, "Optimum number of cascaded cells for high-power medium-voltage AC–DC converters," *IEEE Trans. Emerg. Sel. Topics Power Electron.*, vol. 5, no. 1, pp. 213–232, Mar. 2017.

[32] B. J. Baliga, *Fundamentals of Power Semiconductor Devices*. New York, NY, USA: Springer, 2008.

[33] J. Xu, L. Wang, Y. Li, Z. Zhang, G. Wang, and C. Hong, "A unified MMC reliability evaluation based on physics-of-failure and SM lifetime correlation," *Int. J. Elect. Power Energy Syst.*, vol. 106, pp. 158–168, 2019.

[34] Infineon Technologies AG, "PC and TC diagrams," Infineon Technologies AG, Munich, Germany, Tech. Rep., 2019.

[35] Infineon, "Technical information IGBT modules use of power cycling curves for IGBT 4," Infineon, Neubiberg, Germany, Tech. Rep. AN2010-02, 2012.

[36] A. Abuelnaga, M. Narimani, and A. S. Bahman, "A review on IGBT module failure modes and lifetime testing," *IEEE Access*, vol. 9, pp. 9643–9663, 2021.